IEEE Photonics Journal
An IEEE Photonics Society Publication

Open Access

Dynamic Responses of Cylindrical Whispering Gallery Mode Revealed by Axial Liquid Disturbance

Volume 12, Number 3, June 2020

Hongchun Zhao
Yue Wang
Yihui Wu

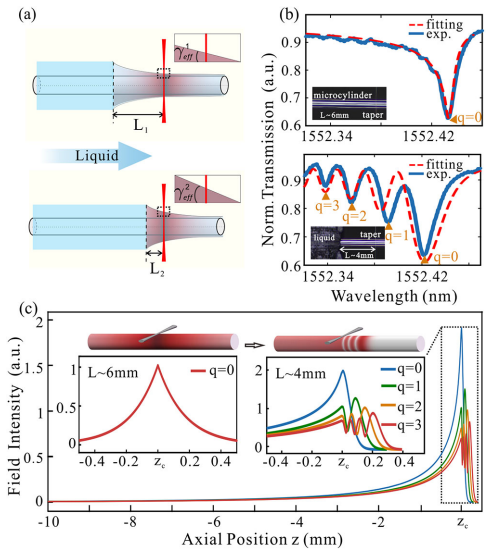

DOI: 10.1109/JPHOT.2020.2998866

Dynamic Responses of Cylindrical Whispering Gallery Mode Revealed by Axial Liquid Disturbance

Hongchun Zhao,[1,2] **Yue Wang**,[1] **and Yihui Wu** [1]

[1]State Key Laboratory of Applied Optics, Changchun Institute of Optics, Fine Mechanics and Physics, Chinese Academy of Sciences, Changchun 130033, China
[2]University of Chinese Academy of Sciences, Beijing 100049, China

DOI:10.1109/JPHOT.2020.2998866

Manuscript received February 12, 2020; revised May 14, 2020; accepted May 27, 2020. Date of publication June 1, 2020; date of current version June 22, 2020. This work was supported by the National Natural Science Foundation of China (NSFC) under Grants 61727813, 61805241, and 61974143. Corresponding authors: Yihui Wu; Yue Wang (e-mail: yihuiwu@ciomp.ac.cn; xiaotianyueyue@gmail.com).

Abstract: Cylindrical whispering gallery mode (WGM) microresonators have achieved much attention in the sensing field due to high sensitivity, compatibility and integration. The excitation of spiral modes in such a resonator is unavoidable, causing the axial field distribution, and the injected analytes will undoubtedly interact with the axial mode field, resulting in unclear spectral responses. Here, these responses of the cylindrical WGM are investigated experimentally and theoretically for the first time. Using an optical fiber as the resonator, the experiment is performed by introducing the liquid into a part of the evanescent field along the axis. The perturbation is attributed to the modification of the resonator's profile, leading to an increase of the effective slope. We find the experimental demonstrations of the short-wavelength oscillations of spectral line shapes and the blue shifts of resonant wavelengths. Theoretical studies are consistent with the experimental phenomena. The research in the responses to the axial perturbation provides valuable insights into the effect of spiral modes on cylindrical WGMs and a potentially powerful tool for real-time biochemical analysis.

Index Terms: Optical microresonator, cylindrical whispering gallery mode, axial mode field, spectral line shape, blue shift.

1. Introduction

Whispering gallery mode (WGM) optical microresonators based on cylindrical geometry including solid cylinders and hollow tubes are very attractive for sensing applications due to their high sensitivity, compatibility with microfluidics and integration on a chip [1]–[3]. Previous studies have shown that, by monitoring mode characteristics such as the spectral positions or widths of the resonance mode, the changes in surrounding refractive index or the binding of biochemical molecules onto the cylindrical microresonator surface can be revealed [4], [5]. Mostly, the near-field tapered fiber coupling method is used to excite the modes due to its high coupling efficiency [6]. It is generally considered that the resonance mode excited in the cylindrical microresonator is identical as that in an optical ring microresonator, that is, the in-plane WGM with zero axial wavevector components propagating along the circumferential direction [7]–[9]. However, due to the lack of axial confinement in the microcylinder and the nonzero axial propagation components

of the excitation light from the tapered fiber, the excitation of spiral modes is unavoidable [10]. Most studies pay more attention to the sensing performance of the in-plane WGM. They believe that the coupling of the in-plane WGM with the excited spiral modes broadens its line shape, causing the inaccurate identification of the resonant wavelength and the loss of sensitivity. Accordingly, some approaches are adopted to reduce the effect of spiral modes on the in-plane WGM, such as by establishing a curve-fitting equation to extract the resonant wavelengths [11] or by coupling with a wider tapered fiber to decrease the appearance of spiral modes [12]. Nevertheless, the fact is that, due to the existence of spiral modes, the excited observable mode, i.e., the cylindrical WGM, is an overlapping mode containing the in-plane WGM and spiral modes, and owns the axial field distribution with several millimeters long. Besides, the analyte for detection is usually introduced through injecting along the axis. Therefore, the interaction between the analyte and the axial mode field will inevitably cause the perturbation of the cylindrical WGM, the influence on the spectral responses remains unclear as well.

In this article, the responses of the cylindrical WGM to the axial disturbance are investigated for the first time. An operable experiment is carried out to emphatically disturb the resulting axial mode field by moving the liquid along the axis to the region where the in-plane WGM localizes. There are two experimental phenomena observed in the process of increasing external refractive index: the indistinguishable resonance dips become distinguishable, and the resonant wavelengths move to shorter wavelengths (blue shift), which cannot be interpreted by the increased effective refractive index in perturbation theory [13]. The explanation is innovatively advanced by attributing the modification of the external refractive index profile along the axis to the cylinder-to-cone transition, and theoretical predictions are consistent with experimental results. The interaction mechanism clarified here provides solutions to better performance of cylindrical resonators, and the research provides a basis for the further development of cylindrical microresonators in the sensing and other fields.

2. Experiment Setup and Spectral Responses

The cylindrical microresonator adopted is fabricated by a section of silica single-mode fiber (Corning, SMF–28) after stripping and cleaning. As shown in Fig. 1(a), a narrow linewidth tunable laser, operated at wavelengths $\lambda\sim$1550 nm, is used to excite cylindrical WGMs via a low-loss tapered fiber with diameter $\sim$2.5 μm, which is prepared by the heat stretching method. The free spectrum range (FSR) of the resonator shown in Fig. 1(b) is about 4.2 nm in approximate agreement with the theoretical FSR, $\lambda^2/(2\pi n_c r_e)$, of the in-plane WGM [15]. Here, the refractive index n_c and the radius r_e of the microcylinder are 1.45 and 62.5 μm, respectively. The periodic pattern of the Lorentzian-like dips is the evidence of the excited cylindrical WGMs. Additionally, the exciting mode, shown in the zoomed region (1551.2–1551.6 nm) of Fig. 1(b), manifests as a skewed Lorentzian line shape. Next, to minimize the introduced absorption losses, considering the extremely low absorption of heavy water around 1550 nm [16], the liquid ($n_s = 1.317$) as the axial disturbance is introduced to cover the outside of the solid microcylinder. It is contained in an open chamber of length 10 mm, width 50 mm and depth 20 mm on a Polymethyl Methacrylate block, which is driven by a stepping motor to indirectly control axial positions of the liquid level. Before the experiment, the whole system and the liquid are put together over 60 minutes for thermal balance.

In experimenting the covering liquid is moved from a distance to the coupling point. For the convenience of description, the axial position at the coupling point is set as the reference point z_c, and the axial position of liquid level is measured by the relative distance L from the coupling point. The transmission spectra at different relative distances are shown in Fig. 1(c). During moving the liquid, at first, the transmission spectrum hardly changes, e.g., $L\sim$6 mm, that is, the cylindrical WGM's line shape maintains asymmetric and broadening. Then when L is further reduced to, e.g., $\sim$2 mm, the line shape has changed and presents the single-side oscillation in the short-wave direction. Besides, all the modes take the blue shift. While the relative distance decreases to $\sim$40 μm, the blue shift stops and the linewidth visibly widens. Subsequently, by further moving the liquid forward, the phenomenon of the red shift occurs. It can be inferred that the final red

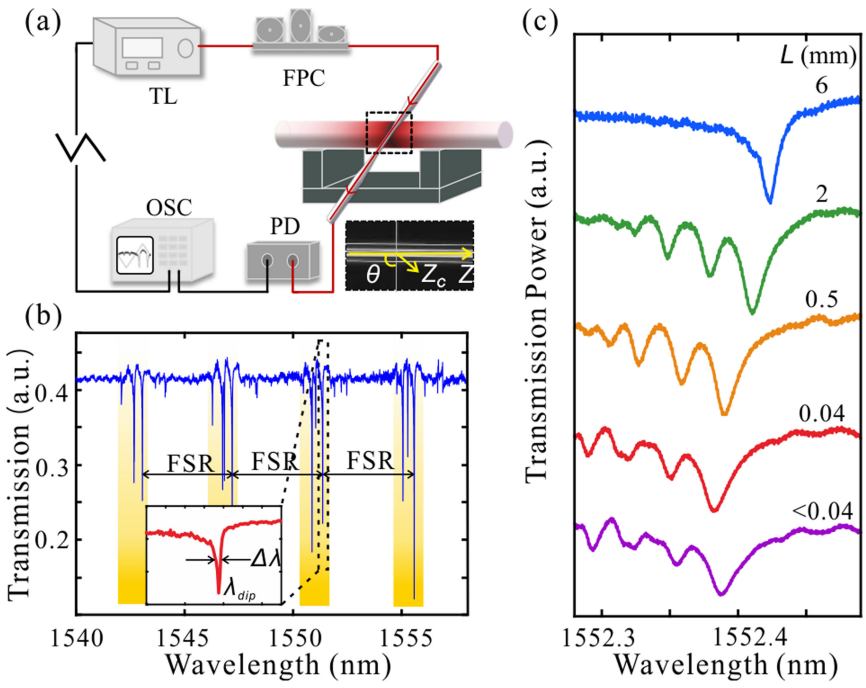

Fig. 1. (a) Schematic diagram of experimental setup before covering the liquid and the microscope image of the microcylinder touched by the tapered fiber perpendicular to its axis at the coupling position z_c. $\theta = 90°$. TL: tunable laser, FPC: fiber polarization controller, PD: photodetector, OSC: oscilloscope. (b) Measured transmission spectrum of the coupling system. The inset shows the typical line shape of the cylindrical WGM with $\lambda_{dip} = 1551.386$ nm and $\Delta\lambda = 0.012$ nm. (c) Transmission spectra after covering the liquid with the relative distance L about 6, 2, 0.5, 0.04 and <0.04 mm.

shift phenomenon is because the perturbation to the in-plane WGM field plays a predominant role, leading to an increase in the effective refractive index of the in-plane WGM [17], and a full discussion of the usual red shift lies beyond the scope of this study. Before that, the key point is that the liquid overlaps with the axial evanescent field rather than the traditional thin ring-like field. Here for brevity, the phrase "axial evanescent field" is used to refer to the partial evanescent field overlapped along the axis. The two abnormal responses of the cylindrical WGM, i.e., the visualization of resonance dips and the blue shifts of resonant wavelengths, are the emphases of our study.

3. Analysis Model and Discussion

Considering that the microcylinder has no axial restriction and the coupling beam from the tapered fiber travels in different directions, the cylindrical WGMs are a set of coupling resonances, containing an in-plane WGM with the resonant wavelength λ_0 and a series of spiral modes with shorter resonant wavelengths [18], [19]. Moreover, the resulting cylindrical WGM field E in the steady state at axial position z_c can be simply expressed as an integral of the fundamental field complex amplitude like $E_0 \exp[i(\beta + i\alpha) \times S(N, z_c)]$ [20]:

$$E(\beta, z_c) = \int_0^{\infty} \frac{dN}{N^{1/2}} E_0 \exp[i(\beta + i\alpha) \times S(N, z_c)], \quad (1)$$

where α is the material attenuation constant, $\beta = 2\pi n_c/\lambda$ is the propagation constant, $1/N^{1/2}$ indicates that the diffraction loss caused by spiral modes in coupling increases with the number

of turns N and so the field amplitude E_0 will be reduced to $E_0/N^{1/2}$, where E_0 is pretreated to unitary in our study for simplicity. $S(N, z_c)$ is the path length of propagating N turns.

Here the accurate expression about $S(N, z_c)$ is the focus under the disturbance of the covering liquid. It is noted that the modification of the effective refractive index n_{eff} along the axis can achieve the cylinder-to-bottle transition [21]. Similarly, we attribute the change in n_{eff} caused by the covering liquid to the modification of microcylinder's profile, i.e., the variation in the effective radius r_{eff} ($r_e \times n_{eff}$) along the axis. The variation is quantitatively described by the effective slope γ_{eff}, termed as $\gamma_{eff} = |\mathrm{d}(r_{eff})|/\mathrm{d}z$. The microcylinder with a small linear variation in the effective radius can be regarded as a microcone with the equivalent effective slope. Consequently, the path length in the effective microcone is express as $S(N, \gamma_{eff}, z_c) \approx 2\pi r_e N - \pi^3 \gamma_{eff}^2 r_e N^3/3 - 2\pi \gamma_{eff} N z_c$, where the effective slope γ_{eff} has replaced the physical slope γ ($|\mathrm{d}r_e|/\mathrm{d}z$) [22].

The resonance mode shows as the observable line shape in the transmission spectra, which is theoretically given by the transmitted power of the cylindrical WGM field over a range of wavelengths as [23],

$$P = 1 + |f|^2|E|^2 + 2|f|\cos\varphi \mathrm{Re}(E) - 2|f|\sin\varphi \mathrm{Im}(E), \tag{2}$$

where f is the transmission-coefficient ratio of the cylindrical WGM field to the input field, and φ is the phase difference between the out-coupling cylindrical WGM field and the transmitted input field. The cylindrical WGMs occur at discrete wavelengths, which satisfy the conditions of constructive self-interference in Eq. (1). The resonant wavelengths related to axial mode number $q = 0, 1, 2, 3, \ldots$ can be simply indicated as [20],

$$\lambda_q \approx -\frac{\lambda_0}{2}\left(\frac{3\pi}{4} + 3\pi q\right)^{2/3}\left(r_e{}^{-2/3}\beta_0{}^{1/3}\gamma_{eff}{}^{2/3}\right)/\beta_0 + \lambda_0, \tag{3}$$

where λ_0 and n_{eff}^0 are the resonant wavelength and the effective refractive index of an in-plane WGM, respectively, $\beta_0 = 2\pi n_{eff}^0/\lambda_0$ is the corresponding propagation constant with zero axial wavevector component. In our experiment, because the physical geometry r_e and the refractive index around the region where the in-plane WGM localizes, i.e., n_{eff}^0, always remain unchanged, λ_0 and β_0 are constant.

In the process that the liquid is moved towards the coupling point, the overlapping area with the axial evanescent field increases, the profile modification thus gets enhanced. That is, as shown in Fig. 2(a), the cylindrical WGM experiences an increase of the effective slope, and this is demonstrated by fitting the experimental spectral line shape of the cylindrical WGM using Eq. (2). Fig. 2(b) shows the fitting results. The transmission spectrum in the upper panel represents the spectral line shape of the cylindrical WGM at $L\sim$6 mm, and the fitting results show $\gamma_{eff} = 8.7 \times 10^{-7}$; The transmission spectrum at $L\sim$4 mm is shown in the lower panel, and the fitting results display $\gamma_{eff} = 1.6 \times 10^{-5}$. From the accurate fitting results, it is found that the covering liquid near the coupling point leads to a great increase of the effective slope γ_{eff}. This has proved the proposed interaction mechanism with the axial evanescent field and achieved the cylinder-to-cone transition. Obviously, the side with a larger effective radius is located on the side covered by the liquid.

According to Eq. (1), the field distribution of the cylindrical WGM with axial mode number q can be easily get. It is noteworthy that the path length is expressed as $S(N, \gamma_{eff}, \mathrm{z}, z_c) \approx 2\pi r_e N - \pi^3 \gamma_{eff}^2 r_e N^3/3 - \pi \gamma_{eff} N(z + z_c) + (z - z_c)^2/(2\pi r_e N)$ when the axial detection position z is introduced. As shown in Fig. 3, in such a "conical microresonator", the field distributions of the cylindrical WGMs with different axial mode numbers, labeled by $q = 0, 1, 2, 3 \ldots$ in Fig. 2(b), exhibit local oscillations and localizations along the narrower side but still show continuous attenuation along the wider side. The axial mode number q corresponds to the number of the nodes in the axial field distribution, and the covered axial region expands with q accordingly. Each cylindrical WGM is the result of the coupling of the in-plane WGM and spiral modes at adjacent resonant wavelengths. The cylindrical WGM with $q = 0$ is predominated by the in-plane WGM with great localization; The high-order q modes are largely dominated by the spiral modes and experience stronger radiation losses, and further their mode localizations are greatly weakened due to the experienced attenuation. The

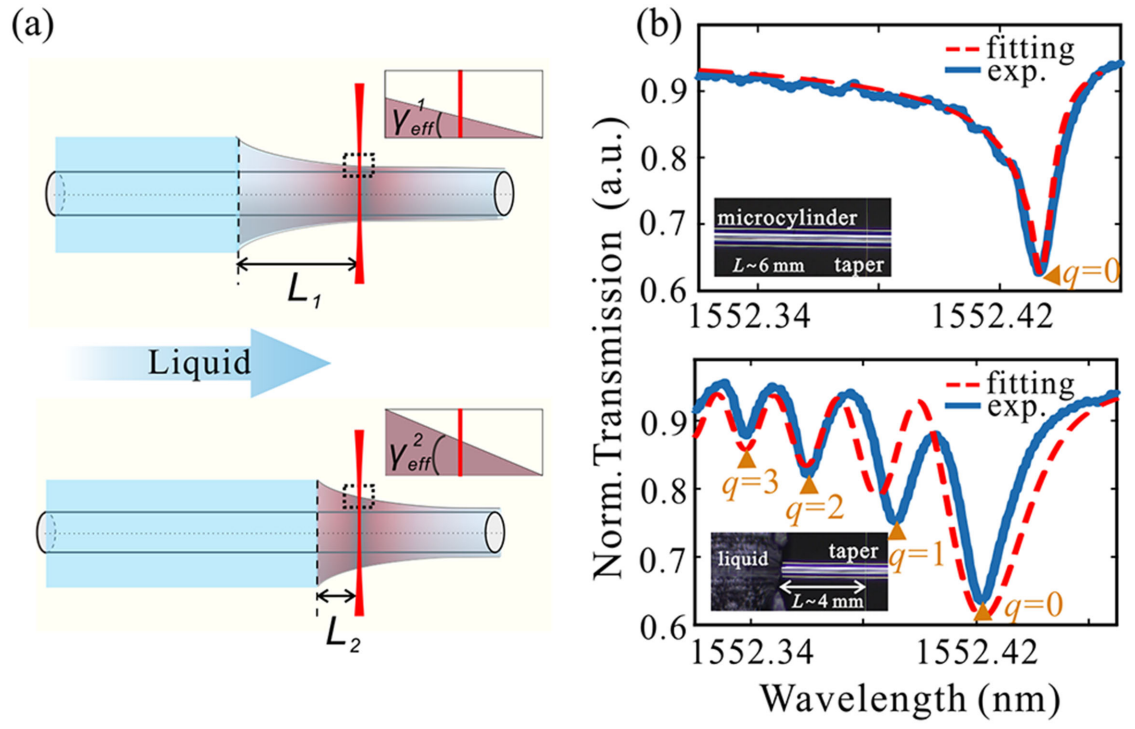

Fig. 2. (a) Equivalent diagram of the moving liquid experiment. $L_1 > L_2$, $\gamma^1_{eff} < \gamma^2_{eff}$. The blue area represents the covering liquid, and the red distribution represents the effective profile of the microcylinder, the deeper the red, the larger the filed amplitude. (b) Transmission spectra with the relative distance L of about 6 mm (upper panel) and about 4 mm (lower panel). In upper panel: $\lambda_{q=0} = 1552.434$ nm, and the fitting parameters are $\lambda_0 = 1552.435$ nm, $f = 0.19$, $\varphi = 2.72$, $\alpha = 1.2 \times 10^{-5}$ μm^{-1}. In lower panel: $\lambda_{q=0} = 1552.422$ nm, $\lambda_{q=1} = 1552.392$ nm, $\lambda_{q=2} = 1552.361$ nm, $\lambda_{q=3} = 1552.339$ nm, and the fitting parameters are $\lambda_0 = 1552.435$ nm, $f = 0.1$, $\varphi = 2.72$, $\alpha = 1.2 \times 10^{-5}$ μm^{-1}.

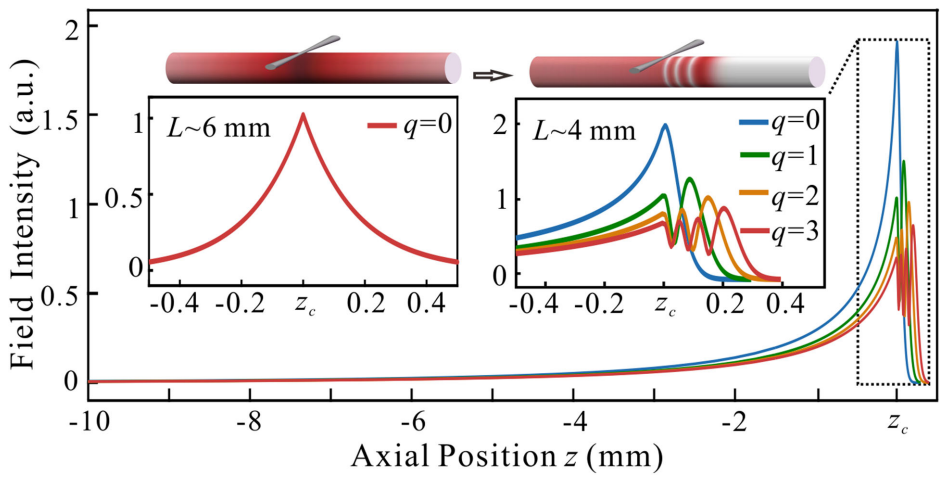

Fig. 3. Axial intensity distributions of the cylindrical WGMs with $q = 0$, 1, 2, and 3 when the relative distance L is about 4 mm. The right inset shows the amplification at the axial position from -0.5 mm to 0.4 mm, and the left inset shows the axial intensity distribution of the cylindrical WGM with $q = 0$ when L is about 6 mm. The above negative sign "$-$" in horizontal ordinate symbolizes the axial positions lying at the wider side of the coupling point.

ability of mode localization, estimated by the absolute transmission power difference between the lowest point and the baseline of its resonant line shape, will decrease with the increasing axial mode number q.

When the liquid is not introduced or the perturbation to the cylindrical WGM is negligible, the field of the mode with $q = 0$ shown in the left inset of Fig. 3 presents the two-sided exponential field distribution, and other distributions of high-order q mode fields are similar to that but hardly localized. Significantly, the cylindrical mode with $q = 0$ behaves as the deepest dip in the transmission spectrum all the time but the others show the indistinguishable resonance dips. However, when the covering liquid successfully perturbs the cylindrical WGMs, as shown in the right inset, the increased effective slope localizes the mode field along the narrower side, and the localization effect is greatly enhanced for low-order q mode. Meanwhile, the loss effect has been suppressed so that the linewidths of the modes get narrower and the exact resonant shapes can be easily resolved. As a result, the appearance of the resonance dips of the high-order q cylindrical WGMs exhibits the oscillation towards the short-wavelength direction. Furthermore, based on theoretical prediction, with the effective slope less than the above fitting value 1.6×10^{-5}, the spectral oscillation still occurs, but the ability of the high-order q mode localization greatly attenuates with the decreased value. The appearance of each observable resonance dip not only depends on the resulting increased effective slope but also the system noise and the spectral resolution, and the field amplitude shown in Fig. 3 maintains close to zero when L is greater than 4 mm, causing a negligible perturbation to the cylindrical WGM. Thus, the oscillation is hardly observed at $L > 4$ mm in our experiment.

Besides, the blue shift can also be interpreted according to Eq. (3). The equation reveals that the resonant wavelength λ_q is inversed to the effective slope γ_{eff}, and the essential contributor for the phenomenon is that the decrease of path length $S(N, \gamma_{eff}, z_c)$. Therefore, the resulting increased effective slope certainly leads to the blue shift of the resonant wavelengths. Then, the relationship between the relative distance L and the resulting γ_{eff} is quantified. Here, we deduce that they present an exponential decay relation according to the following reasons. Firstly, the definition of γ_{eff}, i.e., $|\mathrm{d}r_{eff}|/\mathrm{d}L$, indicates that the relation can be directly determined by the relationship between L and the proportion κ of the axial evanescent field occupied by the liquid from $-\infty$ to $(z_c - L)$ to the total axial evanescent field from $-\infty$ to $+\infty$. It is noteworthy that we have simplified the expression of r_{eff} as $r_e \times \{\eta[\kappa n_s + (1 - \kappa)n_a] + (1 - \eta)n_c\}$, where η represents the proportion of the evanescent field to total cylindrical WGM field, and the refractive index of external air n_a is equal to 1. Here, we think that the introduction of the axial covering liquid causes little change in the proportion of the evanescent field η, but it redistributes the axial mode field as shown in Fig. 3. Based on the definition of κ, so get

$$\kappa \propto \int_{-\infty}^{z_c - L} \left|E(z_c)\right|^2 \mathrm{d}z \Big/ \int_{-\infty}^{+\infty} \left|E(z_c)\right|^2 \mathrm{d}z. \tag{4}$$

The exponential relation can be easily obtained from fitting the expression with the exponential type as $\kappa = a \exp(-bL) + c$, where a, b, and c are the fitting parameters, and all R^2 are greater than 99%. To summarize, the relationship between L and the resulting γ_{eff} can be expressed as,

$$\gamma_{eff} = k\left(r_{eff}^s - r_{eff}^a\right) \exp\left(-kL\right), \tag{5}$$

where r_{eff}^s and r_{eff}^a represent the corresponding effective radii based on the limit conditions when L is close to zero and infinity, k is a fitting parameter determined by the cylindrical WGM field distribution. Besides, the relation of resonant wavelength λ_q to L is further derived as,

$$\lambda_q = -\frac{\lambda_0}{2\beta_0}\left(\frac{3\pi}{4} + 3\pi q\right)^{2/3}\left(r_e^{-2/3}\beta_0^{1/3}\left(\left(r_{eff}^s - r_{eff}^a\right)k\exp\left(-kL\right)\right)^{2/3}\right) + \lambda_0. \tag{6}$$

Hence, Eq. (6) has provided a quantitative description for the blue shift of the resonant wavelength, and the expression as a fitting equation will be compared with the experimental data.

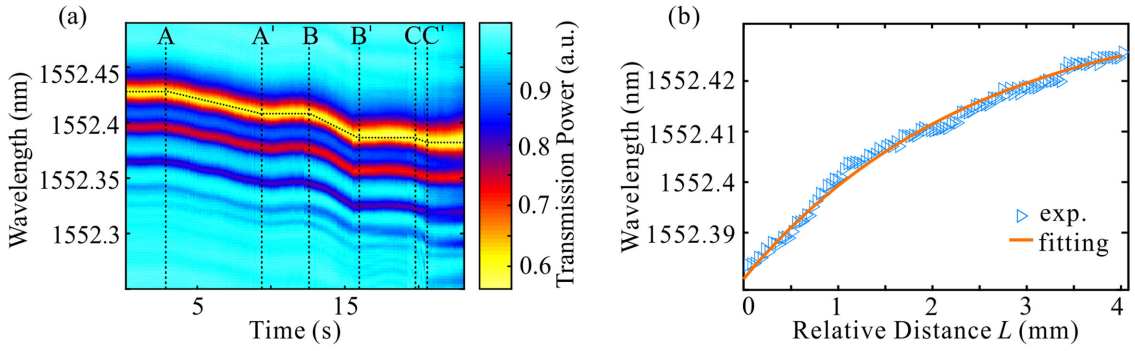

Fig. 4. (a) Colormap of transmission power spectra over time. The data are recorded with a speed of 370 μm/s. Time interval AA', BB', and CC' correspond to the relative distance L of 4000 to 1600 μm, 1600 to 350 μm and 350 to 40 μm. The dashed black curves are plotted to guide the eye. (b) The dependence of the resonant wavelengths of the mode $q = 0$ to the relative distance L. The blue triangles plot the experimental data, and the yellow line is the fitting curve. The fitting parameters are $\lambda_0 = 1552.436$ nm, $k = 6.1\times10^{-4}$ μm^{-1}, $(r^s_{eff} - r^a_{eff})/r^0_{eff} = 0.2\%$, $r^s_{eff} - r^a_{eff} = 0.3$.

To directly prove that the shift of the resonant wavelength is caused by the liquid movement, we adopt a stop-and-go method to move the liquid and record the data at the same time. Fig. 4(a) shows the dependence of transmission spectra on time-varying relative distance L. It is found that all resonant wavelengths take the blue shift as the liquid moves towards the coupling point during the three moving segments AA', BB', and CC'. Take the cylindrical WGM with $q = 0$ as an example, as shown in Fig. 4(b), the dependence of its resonant wavelengths from the three segments on L is fitted well with Eq. (6) with $R^2 = 99.21\%$. The effective slope γ_{eff} at different axial positions can be easily obtained by substituting fitting parameters to Eq. (5), e.g., γ_{eff} increases from 1.6×10^{-5} to 17.9×10^{-5} as L shortens from 4000 μm to 40 μm. It has been proven theoretically and experimentally that, the increased overlap of the axial mode field with the covering liquid leads to the increase of the effective slope and further the blue shift. And the correctness of the established physical model and the fitting equation are verified by the above analyses.

Based on the above observable sensing signal such as the blue-shift or the red shift of the spectral line shape, the change in positions of the axial perturbation can be determined in real-time. Firstly, as is known to all, the field overlap with the axial perturbation will affect the sensitivity, which is an essential figure of merit for the sensors and here defined as: $S = \Delta\lambda_q / \Delta L$. In our configuration, the closer to the coupling point, the larger the overlap. The sensitivity is strongly related to the initial axial distance L_0 to the coupling point. Theoretically, concluded from Eq. (6), the sensitivity shown in Fig. 5(a) approximately increases from 4 pm/mm to 22 pm/mm when L_0 moves from 4 mm to the coupling point. Besides, the blue shifts of the resonance dip $\lambda_{q=0}$ in the time interval AA', BB' and CC' in Fig. 4(a) are also shown in Fig. 5(a), which are fitted well with the theoretical sensitivities. The results present that the perturbation near the coupling point will lead to a stronger interaction and a higher sensitivity.

Then, the approach to increase the proportion of axial mode field on the cylindrical WGM field are also investigated. It is well known that the axial mode field is obviously associated with the nonzero axial wavevector components of the coupling beam, which heavily depend on the tilt angle θ [24]. We repeatedly move the liquid among L~1.35–1.9 mm at different tilt angles. When θ is less than 76°, no resonance dips are observed in the transmission spectrum because of the increase of loss. Fig. 5(b) shows the linear fittings of the resonance shift versus the liquid movement at the five tilt angles, and the sensitivities improve from 17.7 pm/mm to 38.7 pm/mm when the tilt angles decrease from 90° to 76°. The results indicate that decreasing tilt angles offers an efficient way to increase the proportion of axial mode field and improve the sensitivity.

Furthermore, the generality of the above experiments and results is discussed. First, actual depth of interacting with the covering liquid along the radial direction is limited by the depth of

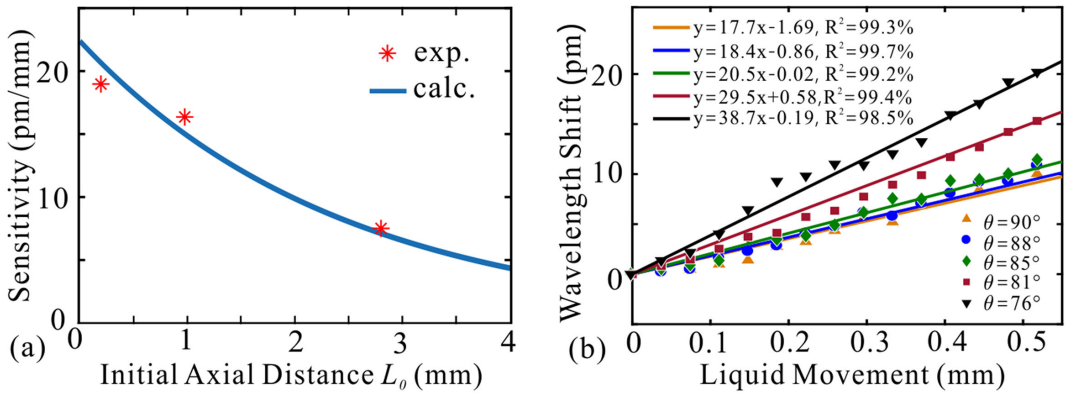

Fig. 5. (a) Dependence of the sensitivity on initial axial distance L_0 for fitting Eq. (6) and the experimental data. (b) Measured shifts of the cylindrical WGM with $q = 0$ versus the liquid movement and their corresponding linear fitting curves for different tilt angles θ.

the evanescent wave, which can be reduced to a cladding layer with uniform thickness t on the order of wavelength λ ($t \ll \lambda$) [25], thus the above conclusions are still applicable when the volume reduces to microfluidic level. Then, the interaction mechanism, i.e., the profile modification of cylindrical-to-cone transition, can be attained not only by the axial change in the external refractive index but also by in the internal refractive index. As a result, all the above results are also available for microfluidic sensing utilizing microcapillary resonators, including liquid-core optical ring resonator and the fluorescent core microcapillary.

4. Conclusion

In summary, this study has revealed the dynamic responses of the cylindrical WGM by moving the liquid to the axial evanescent field and further given a new perspective on the interaction mechanism of the axial mode field with disturbances. The covering liquid leads to the cylindrical WGM experiencing the increase of the effective slope, resulting in the resolved resonant line shape in the spectrum and the blue shift of the resonant wavelength. The research has broken the previous understanding of the deteriorated potentiality of cylindrical microresonators as sensors. Benefiting from the excitation of spiral modes and the resulting axial field distribution, the cylindrical microresonator sensors are promising to give more information such as axial positions of analytes and a more comprehensive understanding of the dynamic processes for microfluidic sensing and capillary flow.

References

[1] Y. N. Zhang, T. Zhou, B. Han, A. Zhang, and Y. Zhao, "Optical bio-chemical sensors based on whispering gallery mode resonators," *Nanoscale*, vol. 10, no. 29, pp. 13832–13856, 2018.
[2] Y. Yin *et al.*, "Water nanostructure formation on oxide probed in situ by optical resonances," *Sci. Adv.*, vol. 5, no. 10, 2019, Art. no. eaax6973.
[3] D. Wang, Z. Wang, A. Lee, L. C. Marr, J. R. Heflin, and Y. Xu, "Highly sensitive nano-aerosol detection based on the whispering-gallery-mode in cylindrical optical fiber resonators," *Aerosol Sci. Tech.*, vol. 50, no. 12, pp. 1366–1374, 2016.
[4] Z. Zhang, W. Morrish, K. Gardner, S. Yang, Y. Yang, and A. Meldrum, "Functional lasing microcapillaries for surface-specific sensing," *Opt. Express*, vol. 27, no. 19, pp. 26967–26978, 2019.
[5] L. Chantada, N. I. Nikolaev, A. L. Ivanov, P. Borri, and W. Langbein, "Optical resonances in microcylinders: response to perturbations for biosensing," *J. Opt. Soc. Amer. B*, vol. 25, no. 8, pp. 1312–1321, 2008.
[6] M. Cai, and K. Vahala, "Highly efficient optical power transfer to whispering-gallery modes by use of a symmetrical dual-coupling configuration," *Opt. Lett.*, vol. 25, no. 4, pp. 260–262, 2000.

[7] I. M. White, H. Oveys, X. Fan, T. L. Smith, and J. Zhang, "Integrated multiplexed biosensors based on liquid core optical ring resonators and antiresonant reflecting optical waveguides," *Appl. Phys. Lett.*, vol. 89, no. 19, 2006, Art. no. 191106.
[8] J. T. Gohring, P. S. Dale, and X. Fan, "Detection of HER2 breast cancer biomarker using the opto-fluidic ring resonator biosensor," *Sens. Actuators B-Chem.*, vol. 146, no. 1, pp. 226–230, 2010.
[9] Q. Chen, X. Zhang, Y. Sun, M. Ritt, S. Sivaramakrishnan, and X. Fan, "Highly sensitive fluorescent protein FRET detection using optofluidic lasers," *Lab Chip*, vol. 13, no. 14, pp. 2679–2681, 2013.
[10] A. Meldrum, and F. Marsiglio, "Capillary-type microfluidic sensors based on optical whispering gallery mode resonances," *Rev. Nanosci. Nanotechnol.*, vol. 3, no. 3, pp. 193–209, 2014.
[11] J. W. Silverstone, S. McFarlane, C. P. K. Manchee, and A. Meldrum, "Ultimate resolution for refractometric sensing with whispering gallery mode microcavities," *Opt. Express*, vol. 20, no. 8, pp. 8284–8295, 2012.
[12] V. Zamora, A. Díez, M. V. Andrés, and B. Gimeno, "Cylindrical optical micro cavities: Basic properties and sensor applications," *Photon. Nanostructures*, vol. 9, no. 2, pp. 149–158, 2011.
[13] I. Teraoka, S. Arnold, and F. Vollmer, "Perturbation approach to resonance shifts of whispering-gallery modes in a dielectric microsphere as a probe of a surrounding medium," *J. Opt. Soc. Amer. B*, vol. 20, no. 9, pp. 1937–1946, 2003.
[14] M. Sumetsky, "Mode localization and the Q-factor of a cylindrical microresonator," *Opt. Lett.*, vol. 35, no. 14, pp. 2385–2387, 2010.
[15] G. C. Righini *et al.*, "Whispering gallery mode microresonators: fundamentals and applications," *Rivista del Nuovo Cimento della Societa Italiana di Fisica*, vol. 34, no. 7, pp. 435–488, 2011.
[16] S. Kedenburg, M. Vieweg, T. Gissibl, and H. Giessen, "Linear refractive index and absorption measurements of nonlinear optical liquids in the visible and near-infrared spectral region," *Opt. Mater. Express*, vol. 2, no. 11, pp. 1588–1611, 2012.
[17] G. C. Righini and S. Soria, "Biosensing by WGM microspherical resonators," *Sensors*, vol. 16, no. 6, 2016, Art. no. 905.
[18] A. W. Poon, R. K. Chang, and J. A. Lock, "Spiral morphology-dependent resonances in an optical fiber: effects of fiber tilt and focused Gaussian beam illumination," *Opt. Lett.*, vol. 23, no. 14, pp. 1105–1107, 1998.
[19] V. Zamora, A. Díez, M. V. Andrés, and B. Gimeno, "Interrogation of whispering-gallery modes resonances in cylindrical microcavities by backreflection detection," *Opt. Lett.*, vol. 34, no. 7, pp. 1039–1041, 2009.
[20] M. Sumetsky, "Localization of light on a cone: theoretical evidence and experimental demonstration for an optical fiber," *Opt. Lett.*, vol. 36, no. 2, pp. 145–147, 2011.
[21] F. Luan, E. Magi, T. Gong, I. Kabakova, and B. J. Eggleton, "Photoinduced whispering gallery mode microcavity resonator in a chalcogenide microfiber," *Opt. Lett.*, vol. 36, no. 24, pp. 4761–4763, 2011.
[22] M. L. Irons, "Geodesics on a cone," [Online]. Available: http://www.rdrop.com/∼half/Creations/Puzzles/cone.geodesics/index.html
[23] Y. Lu, X. Zhu, J. Li, Y. Nie, M. Li, and Y. Song, "Tunable oscillating fano spectra in a fiber taper coupled conical microresonator," *IEEE Photon. J.*, vol. 11, no. 4, Aug. 2019, Art. no. 2200807.
[24] V. Kavungal, G. Farrell, Q. Wu, A. K. Mallik, and Y. Semenova, "A comprehensive experimental study of whispering gallery modes in a cylindrical microresonator excited by a tilted fiber taper," *Microw. Opt. Technol. Lett.*, vol. 60, no. 6, pp. 1495–1504, 2018.
[25] M. Ahmad and L. L. Hench, "Effect of taper geometries and launch angle on evanescent wave penetration depth in optical fibers," *Biosensors Bioelectronics*, vol. 20, no. 7, pp. 1312–1319, 2005.